


Bulk properties of the system formed in U + U collisions at $\sqrt{s_{NN}} = 2.12$ GeV using the jet AA microscopic transport model

Aswini Kumar Sahoo ¹, Xionghong He ², Yasushi Nara ³, and Subhash Singha ²

¹*Department of Physics, Indian Institute of Science Education and Research, Berhampur 760010, India*

²*Institute of Modern Physics Chinese Academy of Sciences, Lanzhou 730000, China*

³*Akita International University, Yuwa, Akita-city 010-1292, Japan*

 (Received 2 November 2023; revised 29 February 2024; accepted 9 April 2024; published 3 May 2024)

The Lanzhou Cooling Storage Ring (CSR) facility is set to conduct experiments involving uranium-uranium collisions at center-of-mass energies ranging from 2.12 to 2.4 GeV. Our investigation is focused on various bulk observables, which include charged particle multiplicity (N_{ch}), average transverse momentum ($\langle p_T \rangle$), initial eccentricity (ϵ_n), and flow harmonics (v_n), for different orientations of U + U collisions within the range of $0^\circ < \theta < 120^\circ$ at $\sqrt{s_{NN}} = 2.12$ GeV ($p_{lab} = 500$ MeV). Among the various collision configurations at this energy, the tip-tip scenario emerged with the highest average charged particle multiplicity, denoted as $\langle N_{ch} \rangle$. Notably, both the second- and third-order eccentricities, $\epsilon_{2,3}$, revealed intricate patterns as they varied with impact parameter across distinct configurations. The tip-tip configuration displayed the most pronounced magnitude of rapidity-odd directed flow (v_1), whereas the body-body configuration exhibited the least pronounced magnitude. Concerning elliptic flow (v_2) near mid-rapidity ($|\eta| < 1.0$), a negative sign is observed for all configurations except for the side-side which exhibited a distinctly positive sign. Within the spectrum of configurations, the body-body scenario displayed the highest magnitude of v_2 . For reaction plane correlated triangular flow (v_3), the body-body configuration emerged with the largest magnitude while the side-side exhibited the smallest magnitude. Our study seeks to establish a fundamental understanding of various U + U collision configurations in preparation for the forthcoming CSR External-target Experiment (CEE).

DOI: [10.1103/PhysRevC.109.054902](https://doi.org/10.1103/PhysRevC.109.054902)

I. INTRODUCTION

Experiments involving heavy-ion collisions are designed to delve into the behavior of strongly interacting matter comprising quarks and gluons, a realm governed by quantum chromodynamics (QCD) [1–6]. Under conditions characterized by low temperature and low density, quarks and gluons are confined within hadrons. A primary objective of heavy-ion collision experiments is the exploration of the QCD phase diagram, which is depicted in the temperature (T) and baryon chemical potential (μ_B) plane. In particular, the Beam Energy Scan (BES) program at the BNL Relativistic Heavy Ion Collider (RHIC) facility is executed by colliding gold nuclei with a center-of-mass energy of $\sqrt{s_{NN}} = 3$ –27 GeV, corresponding to μ_B values spanning about 720–155 MeV. The overarching goal is to investigate the QCD phase diagram and discern potential indicators of a QCD phase transition. Concurrently, the Cooling Storage Ring (CSR) facility, situated within the Lanzhou Institute of Modern Physics, is poised to conduct an experiment called CEE (CSR External-target Experiment) [7–12]. This experiment entails uranium-uranium collisions at $\sqrt{s_{NN}} = 2.12$ –2.4 GeV and is designed to explore the QCD phase diagram under conditions characterized by higher baryon densities and lower temperatures.

The uranium nucleus is of special interest due to its prolate-type deformed shape. Furthermore, different angles between the two colliding U nuclei can lead to special orientations during collisions, such as tip-tip, body-body, and side-side,

discussed in [13]. These special U + U orientations are illustrated in Fig. 1. The difference in initial configurations can lead to different patterns in bulk observables, such as collective flow coefficients. In fact, it is worth noting that U + U collisions have been conducted by the STAR experiment at RHIC at $\sqrt{s_{NN}} = 193$ GeV [14–16]. There have been many attempts to differentiate between initial configurations using experimental measurements and various theoretical models [13,17]. Furthermore, the deformation of the U nucleus presents a very unique chance for investigating nuclear structures, such as quadrupole (β_2) or octupole (β_4) deformations, through relativistic heavy-ion collisions [18–24]. This has been demonstrated at both RHIC and CERN Large Hadron Collider (LHC) energies [25,26]. Indeed, the impact of nuclear deformation has been theoretically examined in heavy-ion collisions occurring at intermediate energy ranges, typically within the range of a few GeV. Particular emphasis has been placed on comprehending the influence of collision geometry, nuclear symmetry energy, and the presence of a deformed neutron skin [27–29]. Moreover, several transport models were quite successful in studying the collective flow at intermediate energies [30–33].

The primary focus of this paper is to study the bulk observables, namely charged particle multiplicity (N_{ch}), average transverse momentum ($\langle p_T \rangle$), initial eccentricity (ϵ_n), and flow harmonics (v_n), for different orientations of U + U collisions at $\sqrt{s_{NN}} = 2.12$ GeV using a transport model. The selections of specific orientations are discussed in the next section.

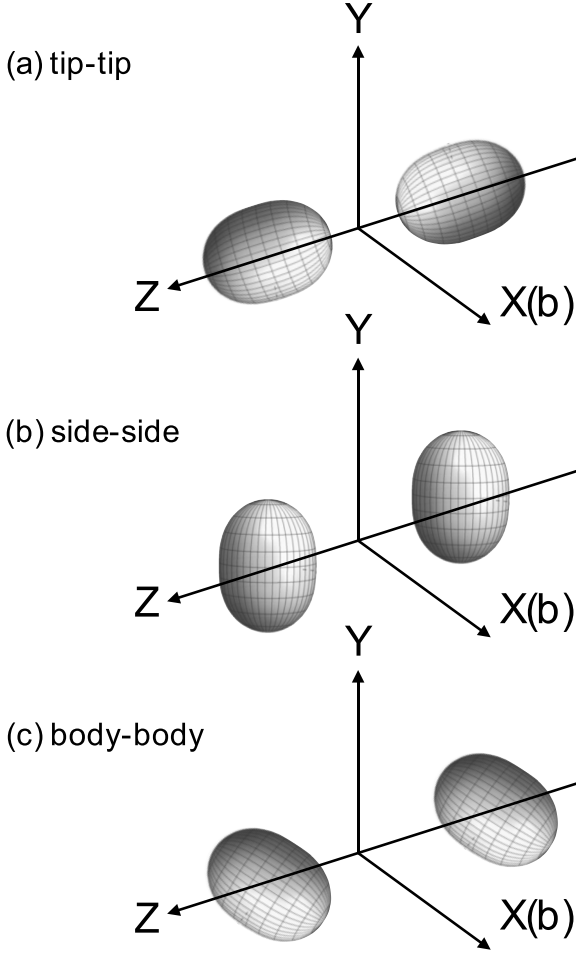


FIG. 1. Schematic diagram of different orientations (tip-tip, side-side, and body-body) of target and projectile nuclei.

II. THE JAM MODEL

In this study, we employ the jet AA microscopic transport model (JAM), a specialized hadronic transport model designed for the simulation of relativistic nuclear collisions [34–40]. The model initiates the simulation by randomly determining the initial positions of each nucleon, drawing from the distribution of nuclear density. In this model, the nucleon density distribution of the uranium nucleus is parametrized by a deformed Woods-Saxon profile [41],

$$\rho = \frac{\rho_0}{1 + \exp[(r - R')/a]}, \quad (1)$$

$$R' = R_0[1 + \beta_2 Y_2^0(\theta) + \beta_4 Y_4^0(\theta)], \quad (2)$$

where ρ_0 represents the standard nuclear density, R' signifies the nuclear radius, a stands for the surface diffuseness parameter, and $Y_l^m(\theta)$ denotes spherical harmonics. In our analysis, we have adopted specific values: $R_0 = 6.802$ fm and $a = 0.54$ fm. The parameters β_2 and β_4 correspond to the quadrupole and octupole deformations of U nuclei, respectively, with values set at 0.28 and 0.093 [17]. Subsequent nuclear collisions are represented as the cumulative outcome of independent binary interactions between hadrons. Consequently, JAM

TABLE I. The polar angle ($\theta_{t,p}$) and azimuth angle ($\phi_{t,p}$) relative to the nucleus's symmetry axis for both the projectile and target nuclei for different orientation of uranium nuclei used in this JAM simulation.

Orientation	θ_p	ϕ_p	θ_t	ϕ_t
tip-tip	0	0–2 π	0	0–2 π
body-body	$\pi/2$	0	$\pi/2$	0
side-side	$\pi/2$	$\pi/2$	$\pi/2$	$\pi/2$
general	0– π	0–2 π	0– π	0–2 π

encompasses the entire process, from the initial phase to the final state interactions within the hadronic gas phase. JAM offers two distinct modes: the cascade mode [34–36] and the mean-field mode [37–40]. In the cascade mode, each individual hadron is advanced in a manner analogous to its behavior in a vacuum, moving freely until it encounters other hadrons and experiences collisions. On the other hand, the mean-field mode incorporates nuclear equation-of-state effects through a momentum-dependent potential that influences the propagation of particles. Utilizing the mean-field approach, calculations have effectively explained the flow measurements from low-energy Au + Au collisions at RHIC, while the cascade mode proved inadequate in reproducing the experimental results. We employ JAM in its mean-field mode [39]: the relativistic quantum molecular dynamics based on the relativistic mean-field (RQMD-RMF), where we use the MD2 equation of state (EoS) [39]. The MD2 EoS has the nuclear incompressibility parameter $K = 380$ MeV, which successfully explains flow measurements at lower RHIC [42] and HADES [43] energies. In the JAM simulation, we have set the evolution time to 50 fm/c, using a time step of 1 fm/c. We have checked that results remain consistent when employing JAM up to 100 fm/c, except in cases of peripheral collisions. In the peripheral bins, we observed changes in results, likely stemming from prolonged interactions among particles in spectator-dominated regions ($|\eta| > 1.0$) compared to the participant-dominated regions near mid-rapidity ($|\eta| < 0.5$). This is an interesting feature that can emerge in heavy ion collisions at an intermediate energy range, where the interaction between spectators and participants plays a significant role [44,45]. This aspect will be investigated in future work.

To select different angular orientations of the uranium nucleus, we vary the polar angle ($\theta_{t,p}$) and the azimuthal angle ($\phi_{t,p}$) relative to the nucleus's symmetry axis for both the projectile and target nuclei. Here, the subscripts t and p stand for the projectile and target, respectively. These orientations are categorized as tip-tip, body-body, and side-side, as detailed in Table I (see Fig. 1). The configuration categorized as general allows all possible orientations of $\theta_{t,p}$ and $\phi_{t,p}$, which is similar to conditions in real experiments.

III. RESULTS AND DISCUSSION

We perform JAM simulations comprising approximately 10^6 events for each of the previously mentioned configurations, covering an impact parameter range from 0.0 to 15.0 fm.

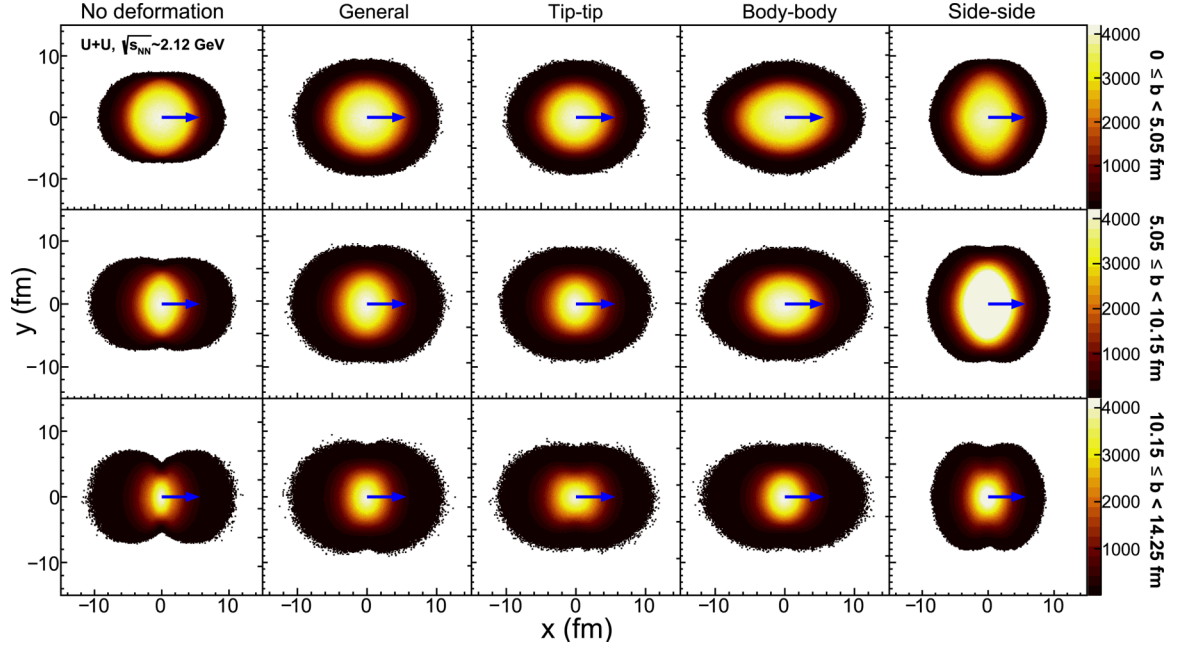


FIG. 2. Transverse profile of (x vs y) of participant nucleons for different orientations (tip-tip, side-side, body-body, and general) of target and projectile uranium nuclei at different impact parameters with deformation for central, mid-central, and peripheral collisions. Results from no deformation are also shown. The arrow indicates the direction of impact parameter.

Figure 2 shows the transverse profile (x vs y) of participating nucleons in different configurations (tip-tip, side-side, body-body, and general) with deformation. Results are also shown without nuclear deformation. The arrows indicate the direction of impact parameter. Figure 3 illustrates the variation in the average number of participating nucleons ($\langle N_{\text{part}} \rangle$) as a function of impact parameter. The $\langle N_{\text{part}} \rangle$ values are also tabulated in Table II. Within the array of configurations studied, it is noteworthy that the body-body scenario exhibits the highest $\langle N_{\text{part}} \rangle$ values, while conversely the side-side configuration demonstrates the lowest values. The tip-tip and general configurations fall between these two extremes.

Within the JAM framework, the initial geometric eccentricities of various configurations can be calculated from the

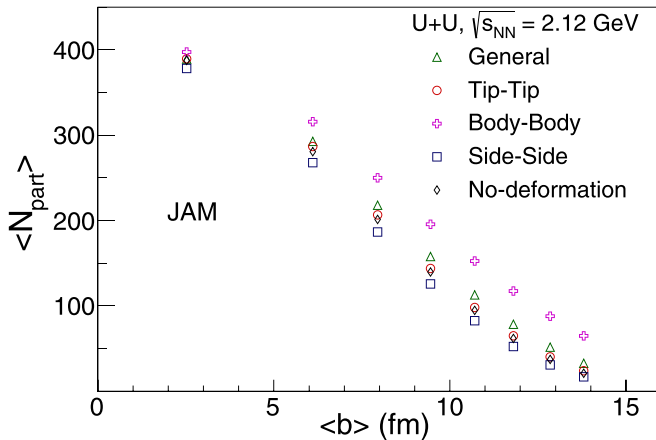


FIG. 3. Average of participating nucleons ($\langle N_{\text{part}} \rangle$) as a function of impact parameter in U + U collisions at $\sqrt{s_{NN}} = 2.12$ GeV for different orientations of colliding nuclei from the JAM model.

participating nucleons following [46]

$$\epsilon_n = \frac{\sqrt{\langle r^2 \cos(n\phi_{\text{part}}) \rangle^2 + \langle r^2 \sin(n\phi_{\text{part}}) \rangle^2}}{\langle r^2 \rangle}, \quad (3)$$

where r and ϕ_{part} are the polar coordinates of participating nucleons in JAM. The angular brackets, $\langle \rangle$, signify that we compute averages within each event. The top and bottom panels in Fig. 4 depict the variations of ϵ_2 and ϵ_3 , respectively, stemming from different orientations as functions of impact parameter. Regarding ϵ_2 , an intricate pattern emerges. Specifically, the side-side configuration exhibits the most substantial magnitude. The body-body configuration showcases a nonmonotonic trend, while the tip-tip and unconstrained configurations follow a similar trajectory. In the case of ϵ_3 , all orientations manifest a consistent increase from central to peripheral collisions, with a distinct ordering pattern pronounced in mid-central and peripheral collisions: side-side $>$ tip-tip $>$ general $>$ body-body.

TABLE II. Average of participating nucleons ($\langle N_{\text{part}} \rangle$) in U+U collisions at $\sqrt{s_{NN}} = 2.12$ GeV for different orientations of colliding nuclei from the JAM model.

$\langle b \rangle$ (fm)	general	tip-tip	body-body	side-side
2.52	389.07	389.70	397.57	378.37
6.1	292.90	286.92	315.75	267.81
7.95	217.90	206.52	250.18	186.65
9.45	158.04	143.81	195.80	125.81
10.7	113.00	98.26	152.58	82.86
11.8	78.68	65.07	117.7	52.56
12.85	51.84	40.53	88.20	30.74
13.8	32.85	24.35	64.86	17.16

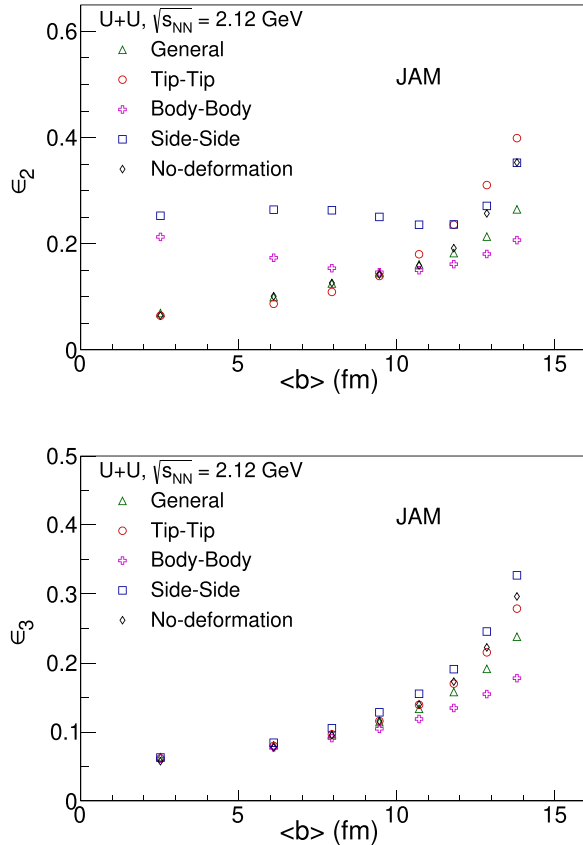


FIG. 4. Eccentricity of participant nucleons (ϵ_2) as a function of impact parameter in U + U collisions at $\sqrt{s_{NN}} = 2.12$ GeV for different orientations of colliding nuclei using the JAM model.

The top panel in Fig. 5 shows the charged particle multiplicity distributions (N_{ch}) from different orientations of U + U collisions. Largely, the pattern is the same for all configurations except body-body. The maximum value of N_{ch} is attained in tip-tip configuration. The bottom panel in Fig. 5 presents the pseudorapidity density ($dN_{ch}/d\eta$) distribution of charged particles in central ($0.0 < b < 5.05$ fm) U + U collisions for different orientations. Among different configurations, there is no appreciable change in the shape of $dN_{ch}/d\eta$.

The top panel in Fig. 6 displays the averaged transverse momentum of all charged particles as a function of the impact parameter. The centrality-related trends appear to be consistent across all configurations, with one notable exception: in mid-central collisions, the body-body configuration exhibits an enhanced $\langle p_T \rangle$ in comparison to the rest of the configurations. This observation is quite unexpected. In fact, the $\langle p_T \rangle$ is found to be higher in the tip-tip configuration compared to other orientations of U + U nuclei at $\sqrt{s_{NN}} = 200$ GeV [13], and this can be attributed to the smaller transverse size and larger binary collisions in this configuration. In order to comprehend our observation, we studied $\langle p_x \rangle$ and $\langle p_y \rangle$ for various orientations and presented in middle and bottom panels in Fig. 6. Our findings reveal that $\langle p_y \rangle$ is consistently larger in body-body configurations compared to other setups. This observation is also substantiated by another intriguing result, which shows that the magnitude of $v_2(\eta)$ in the body-body

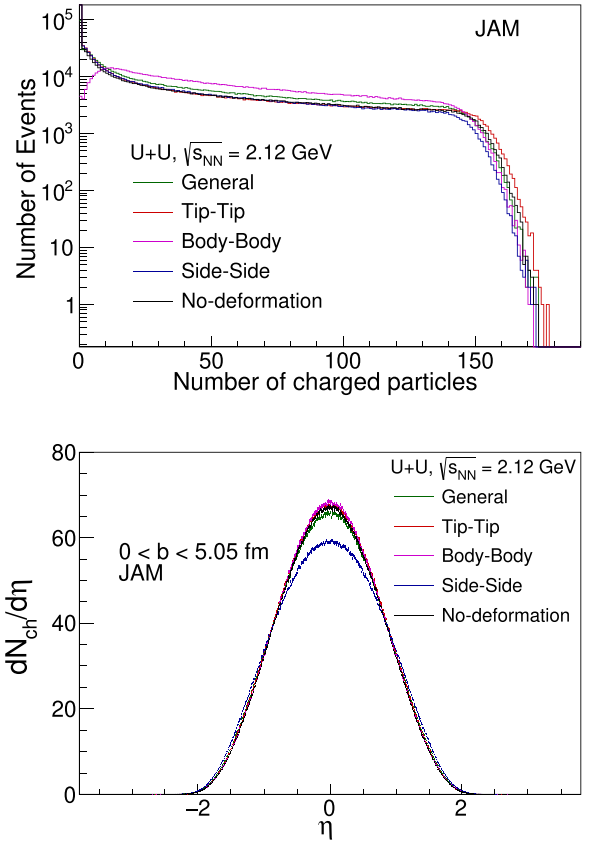


FIG. 5. Top: Probability distribution of the total number of charged particles (N_{ch}) in U + U collisions at $\sqrt{s_{NN}} = 2.12$ GeV for different orientations of colliding nuclei from JAM model. Bottom: Pseudorapidity density distribution of charged particles ($dN_{ch}/d\eta$) in U + U collisions at $\sqrt{s_{NN}} = 2.12$ GeV for different orientations of colliding nuclei using the JAM model.

configuration (shown in Fig. 8) is the most negative, likely as a consequence of enhanced nuclear shadowing. Next we calculate the flow harmonics (v_n) which is defined by [47,48]

$$v_n = \langle \langle \cos n(\phi - \Psi_{RP}) \rangle \rangle, \quad (4)$$

where ϕ is the azimuthal angle of the produced particles and Ψ_{RP} is the true reaction plane. The v_n is averaged over all events and all particles. In JAM simulation, the reaction plane is along the impact parameter direction, hence $\Psi_{RP} = 0$. However, in actual experiments, flow coefficients (v_n) are computed utilizing a reconstructed event plane derived from the final state particles. We have confirmed the consistency of v_n values between the true reaction plane and the experimental method of event plane reconstruction. The top and bottom panels of Fig. 7 show the rapidity-odd directed flow (v_1) of charged particles as a function of p_T and η for minimum bias U + U collisions at $\sqrt{s_{NN}} = 2.12$ GeV. The tip-tip configuration displays the largest v_1 slope, while the body-body configuration displays the smallest slope.

The top and bottom panels of Fig. 8 present the elliptic flow (v_2) of charged particles as a function of p_T and η . The elliptic flow (v_2) displays a notably intricate pattern that varies across different U + U configurations. Typically, within this

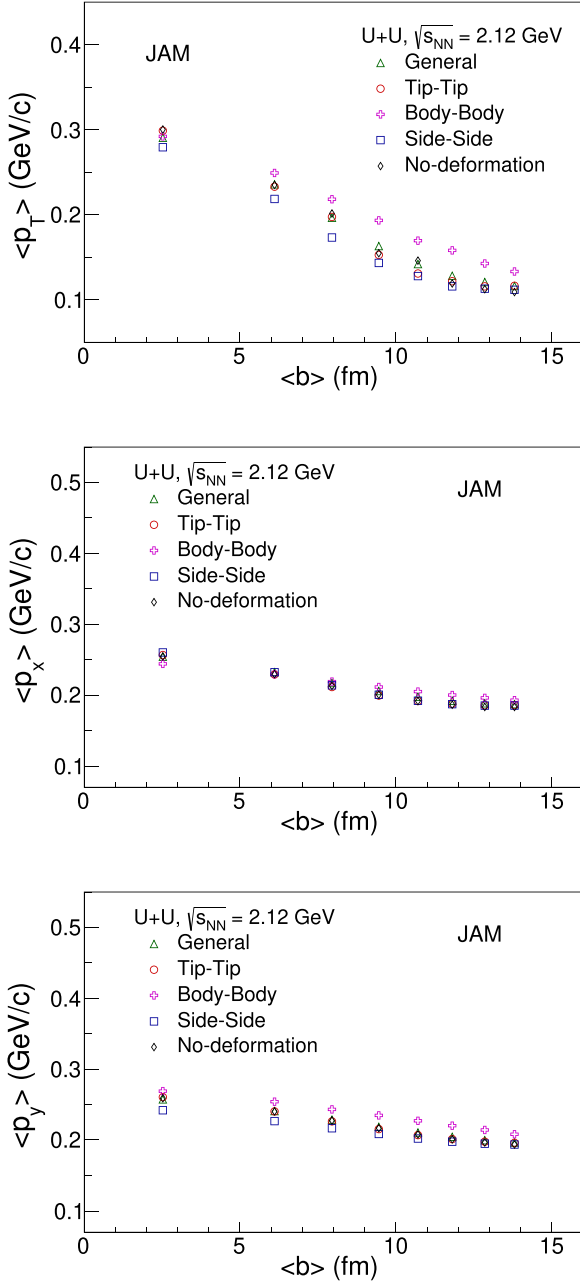


FIG. 6. Average momentum of charged particles ($\langle p_T \rangle$, $\langle p_x \rangle$, and $\langle p_y \rangle$) in U + U collisions at $\sqrt{s_{NN}} = 2.12$ GeV for different orientations of colliding nuclei using the JAM model.

range of beam energy, the sign of v_2 is negative, primarily due to the dominance of in-plane flow over out-of-plane flow, which is caused by shadowing from the spectators. Near mid-pseudorapidity, such negative v_2 trend is particularly pronounced in the general configurations, including tip-tip and side-side. However, there is a distinct departure from this pattern in the case of the side-side configuration, where there is a marked shift with a positive sign for v_2 . This is a very striking observation; in the future event-shape engineering technique will be employed to explore the possibility of disentangling side-side configurations from an unbiased case.

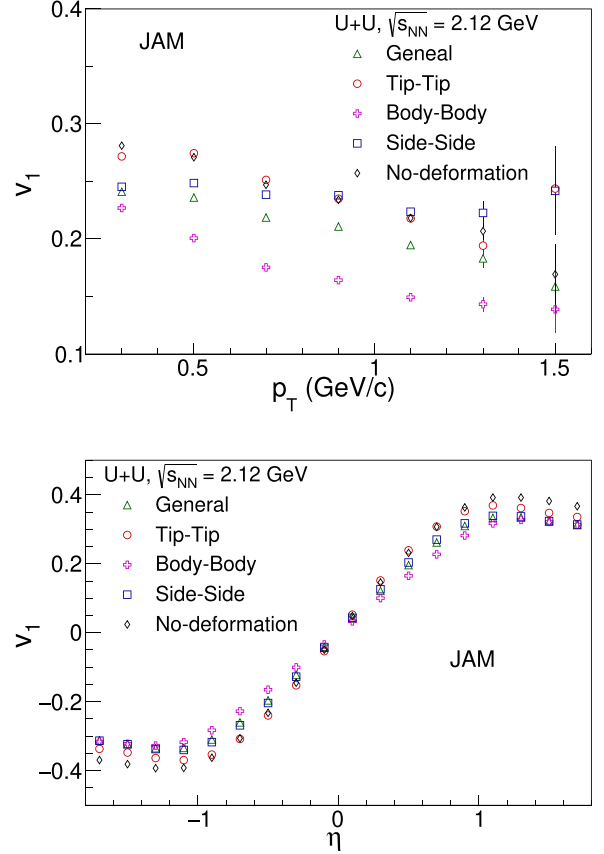
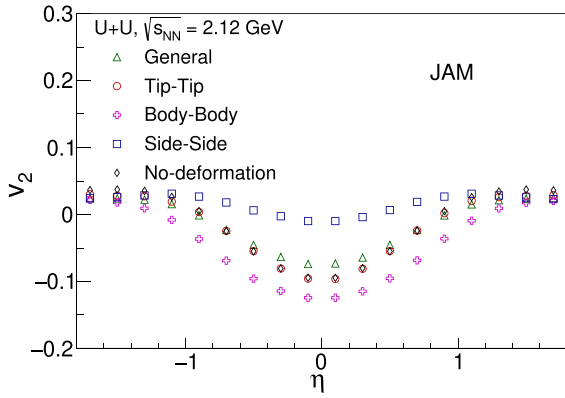
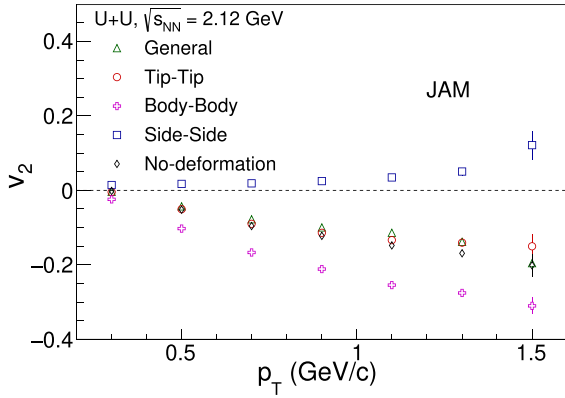
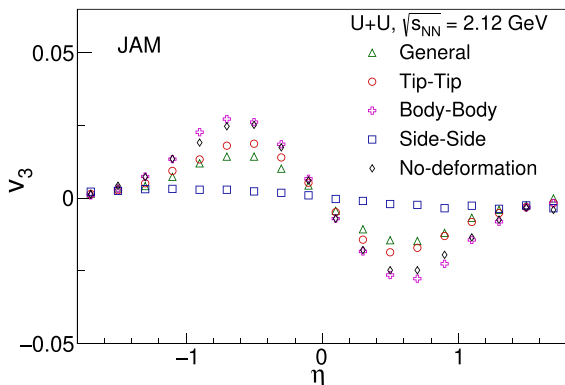
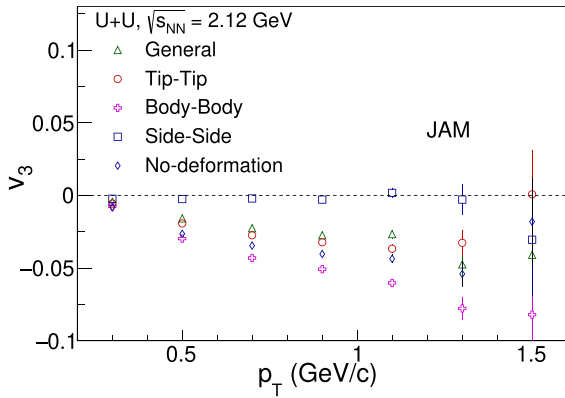
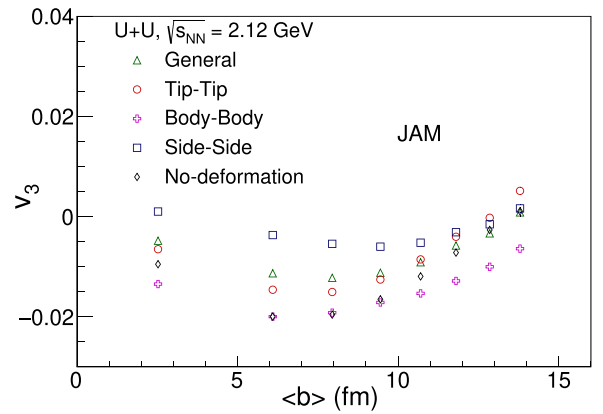
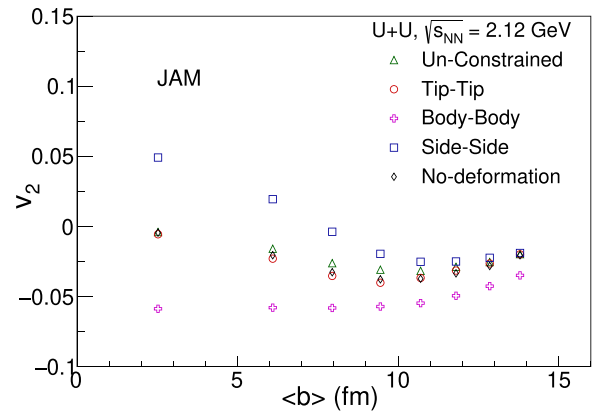
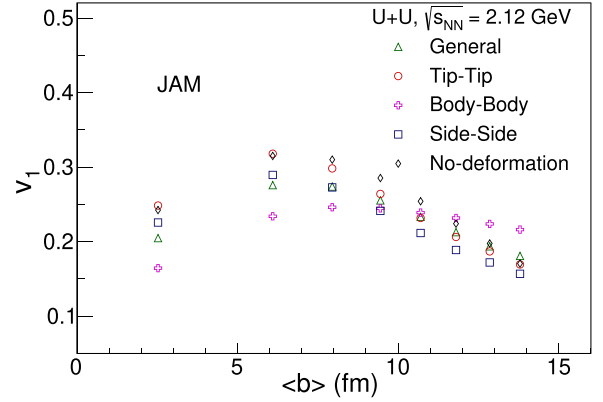


FIG. 7. Directed flow (v_1) of charged particles as a function of p_T (top panel) and η (bottom panel) in minimum bias U + U collisions at $\sqrt{s_{NN}} = 2.12$ GeV for different orientations of colliding nuclei using the JAM model.

The HADES experiment [49], followed by the STAR experiment [50], identified a distinct and substantial negative value for the magnitude of v_3 of protons relative to the reaction plane. Such v_3 is found to be anticorrelated with v_1 , and its origin is expected to be from the triangular shape of the participant nucleons as a combined effect from stopping and nuclear geometry. JAM simulations suggested that a mean-field potential is required to describe STAR v_3 results [50]. In Fig. 9, the top and bottom panels illustrate the v_3 correlated with the reaction plane, as a function of p_T and η . Our observations reveal a substantial v_3 when the system is in a body-body configuration, displaying the highest magnitude, while it is notably smaller in the side-side configuration.

The top, middle, and bottom panels in Fig. 10 present the impact parameter dependence of $\langle p_T, y \rangle$ integrated v_1 , v_2 , and v_3 respectively (the sign of rapidity is weighted for v_1 and v_3 in the integration). A strong dependence of v_n on $\langle b \rangle$ is observed for all U + U orientations. Notably, a distinct pattern emerges for v_1 in the body-body configuration, with the lowest values observed in the most central collisions and the highest values in the most peripheral collisions. Conversely, the side-side configuration exhibits the smallest values in the peripheral bins. Across all impact parameters, the magnitude of v_2 is consistently higher in the side-side configuration compared to the body-body configuration, which consistently

FIG. 8. Same as Fig. 7 but for elliptic flow (v_2).FIG. 9. Same as Fig. 7 but for triangular flow (v_3).FIG. 10. $v_{1,2,3}$ as a function of impact parameter in U + U collisions at $\sqrt{s_{NN}} = 2.12$ GeV for different orientations of colliding nuclei using the JAM model.

displays the lowest magnitude. In the case of the most central collisions, the magnitude of v_3 is maximum in the side-side configuration, while it remains lowest in the body-body configuration. In peripheral collisions, the magnitude of v_3 in the body-body configuration continues to be lower, while no clear distinction can be made for the other configurations.

To disentangle the influence of the initial spatial configuration, we examine the ratio v_n/ϵ_n . Figure 11 consist of two panels, depicting the behavior of v_2/ϵ_2 and v_3/ϵ_3 in relation to the impact parameter. While a complex pattern emerges in the case of v_2/ϵ_2 , the behavior of v_3/ϵ_3 scales perfectly with the expectation from the initial geometric pattern.

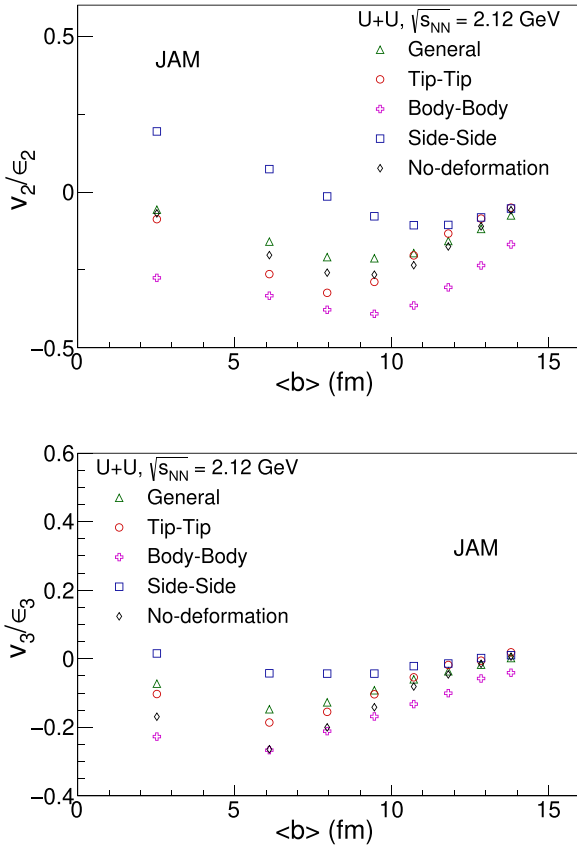


FIG. 11. v_2/ϵ_2 and v_3/ϵ_3 as a function of impact parameter in U + U collisions at $\sqrt{s_{NN}} = 2.12$ GeV for different orientations of colliding nuclei using the JAM model.

IV. SUMMARY AND CONCLUSION

In summary, we have studied charged particle multiplicity, average $\langle p_T \rangle$, and flow harmonics ($v_{1,2,3}$) for different

orientations of deformed uranium on uranium collisions at Lanzhou-CSR energy $\sqrt{s_{NN}} = 2.12$ GeV employing the JAM transport model. Among the various orientation setups at this energy level, the tip-tip scenario stood out with the highest average charged particle multiplicity. Notably, as we explored different configurations, the second- and third-order eccentricities, $\epsilon_{2,3}$, revealed complex patterns in their variations with impact parameters. On the flow harmonics, specifically in the tip-tip configuration, v_1 exhibited the most significant positive magnitude, while, in the body-body configuration, it showed the least pronounced magnitude. When it comes to v_2 , all configurations except the side-side displayed a negative sign consistent with the expectation from dominant in-plane flow compared to out-of-plane. On the other hand, side-side configuration uniquely displayed a positive sign for v_2 . The eccentricity scaled v_2 shows a rich pattern as a function of collision centrality. When looking at individual v_3 and v_3/ϵ_3 , there is significant dependency observed across the different orientation scenarios. Our study will provide a baseline understanding of different configurations of U + U collisions at the upcoming CEE experiment. In a prior study [18], a linear correlation between $\langle v_2^2 \rangle$ ($\langle \epsilon_2^2 \rangle$) and quadrupole deformation (β_2^2) is established in Au + Au collisions at 200 GeV. It facilitates the extraction of β_2 in heavy-ion collisions. In our forthcoming work, we intend to explore these associations by systematically varying the β_2 values within JAM simulations at intermediate energy ranges. Additionally, we plan to employ event-shape engineering techniques to distinguish particular U + U collision orientations from unbiased scenarios.

ACKNOWLEDGMENTS

Financial assistance from Chinese Academy of Sciences (Grant No. XDB34000000) is gratefully acknowledged. We would like to thank our colleagues at the Institute of Modern Physics for many insightful discussions.

- [1] J. Adams (STAR Collaboration) *et al.*, *Nucl. Phys. A* **757**, 102 (2005).
- [2] K. Adcox (PHENIX Collaboration) *et al.*, *Nucl. Phys. A* **757**, 184 (2005).
- [3] I. Arsene (BRAHMS Collaboration) *et al.*, *Nucl. Phys. A* **757**, 1 (2005).
- [4] J. W. Harris and B. Muller, *Annu. Rev. Nucl. Part. Sci.* **46**, 71 (1996).
- [5] B. Müller, J. Schukraft, and B. Wyslouch, *Annu. Rev. Nucl. Part. Sci.* **62**, 361 (2012).
- [6] P. Braun-Munzinger and J. Stachel, *Nature (London)* **448**, 302 (2007).
- [7] D. Hu *et al.*, *Eur. Phys. J. C* **80**, 282 (2020).
- [8] S. H. Zhu, H. B. Yang, H. Pei, C. X. Zhao, X. Q. Li, and G. M. Huang, *J. Instrum.* **16**, P08014 (2021).
- [9] H.-L. Wang *et al.*, *Nucl. Sci. Tech.* **33**, 36 (2022).
- [10] L.-K. Liu, H. Pei, Y.-P. Wang, Y. Wang, B. Zhang, N. Xu, S.-S. Shi, and S. Shi, *Nucl. Sci. Tech.* **34**, 100 (2023).
- [11] B. Zhang, L.-K. Liu, H. Pei, S.-S. Shi, N. Xu, and Y.-P. Wang, *Nucl. Sci. Tech.* **34**, 176 (2023).
- [12] D. Guo *et al.*, *Eur. Phys. J. A* **60**, 36 (2024).
- [13] M. R. Haque, Z.-W. Lin, and B. Mohanty, *Phys. Rev. C* **85**, 034905 (2012).
- [14] L. Adamczyk (STAR Collaboration) *et al.*, *Phys. Rev. Lett.* **115**, 222301 (2015).
- [15] M. Abdallah (STAR Collaboration) *et al.*, *Phys. Rev. C* **103**, 064907 (2021).
- [16] M. S. Abdallah (STAR Collaboration) *et al.*, *Phys. Rev. C* **107**, 024901 (2023).
- [17] M. R. Haque, M. Nasim, and B. Mohanty, *J. Phys. G* **46**, 085104 (2019).
- [18] G. Giacalone, J. Jia, and C. Zhang, *Phys. Rev. Lett.* **127**, 242301 (2021).
- [19] J. Jia, S. Huang, and C. Zhang, *Phys. Rev. C* **105**, 014906 (2022).
- [20] J. Jia, *Phys. Rev. C* **105**, 044905 (2022).
- [21] J. Jia, G. Giacalone, and C. Zhang, *Phys. Rev. Lett.* **131**, 022301 (2023).
- [22] M. Nie, C. Zhang, Z. Chen, L. Yi, and J. Jia, *Phys. Lett. B* **845**, 138177 (2023).
- [23] C. Zhang, S. Bhatta, and J. Jia, *Phys. Rev. C* **106**, L031901 (2022).

- [24] N. Magdy, *Eur. Phys. J. A* **59**, 64 (2023).
- [25] G. Aad (ATLAS Collaboration) *et al.*, *Phys. Rev. C* **107**, 054910 (2023).
- [26] J. Jia, Contribution to the VIth International Conference on the Initial Stages of High-Energy Nuclear Collisions, Initial Stages (unpublished), <https://indico.cern.ch/event/854124/contributions/4135480/>.
- [27] J. Xu, Z. Martinot, and B.-A. Li, *Phys. Rev. C* **86**, 044623 (2012).
- [28] L.-M. Liu, J. Xu, and G.-X. Peng, *Phys. Lett. B* **838**, 137701 (2023).
- [29] X.-H. Fan, Z.-X. Yang, P.-H. Chen, S. Nishimura, and Z.-P. Li, *Phys. Rev. C* **108**, 034607 (2023).
- [30] B.-A. Li, C. M. Ko, A. T. Sustich, and B. Zhang, *Phys. Rev. C* **60**, 011901(R) (1999).
- [31] J. Mohs, M. Ege, H. Elfner, and M. Mayer (SMASH Collaboration), *Phys. Rev. C* **105**, 034906 (2022).
- [32] T. Reichert, J. Steinheimer, C. Herold, A. Limphirat, and M. Bleicher, *Eur. Phys. J. C* **82**, 510 (2022).
- [33] T. Reichert, O. Savchuk, A. Kittiratpattana, P. Li, J. Steinheimer, M. Gorenstein, and M. Bleicher, *Phys. Lett. B* **841**, 137947 (2023).
- [34] Y. Nara, N. Otuka, A. Ohnishi, K. Niita, and S. Chiba, *Phys. Rev. C* **61**, 024901 (1999).
- [35] T. Hirano and Y. Nara, *Prog. Theor. Exp. Phys.* **2012**, 01A203 (2012).
- [36] T. Hirano, P. Huovinen, K. Murase, and Y. Nara, *Prog. Part. Nucl. Phys.* **70**, 108 (2013).
- [37] M. Isse, A. Ohnishi, N. Otuka, P. K. Sahu, and Y. Nara, *Phys. Rev. C* **72**, 064908 (2005).
- [38] Y. Nara and H. Stoecker, *Phys. Rev. C* **100**, 054902 (2019).
- [39] Y. Nara, T. Maruyama, and H. Stoecker, *Phys. Rev. C* **102**, 024913 (2020).
- [40] Y. Nara and A. Ohnishi, *Phys. Rev. C* **105**, 014911 (2022).
- [41] K. Hagino, N. W. Lwin, and M. Yamagami, *Phys. Rev. C* **74**, 017310 (2006).
- [42] M. S. Abdallah (STAR Collaboration) *et al.*, *Phys. Lett. B* **827**, 136941 (2022).
- [43] P. Parfenov, *Particles* **5**, 561 (2022).
- [44] A. D. Sood and R. K. Puri, *Int. J. Mod. Phys. E* **15**, 899 (2006).
- [45] S. Kumar, Y. G. Ma, and G. Q. Zhang, *Phys. Rev. C* **86**, 044616 (2012).
- [46] B. Alver and G. Roland, *Phys. Rev. C* **81**, 054905 (2010); **82**, 039903(E) (2010).
- [47] J.-Y. Ollitrault, *Phys. Rev. D* **46**, 229 (1992).
- [48] A. M. Poskanzer and S. A. Voloshin, *Phys. Rev. C* **58**, 1671 (1998).
- [49] J. Adamczewski-Musch (HADES Collaboration) *et al.*, *Phys. Rev. Lett.* **125**, 262301 (2020).
- [50] M. I. Abdulhamid (STAR Collaboration) *et al.*, *Phys. Rev. C* **109**, 044914 (2024).